Journal of Materials Chemistry A

Accepted Manuscript

ROYAL SOCIETY OF CHEMISTRY

www.rsc.org/materialsA

ARTICLE TYPE www. rsc.org/xxxxxx | XXXXXXXX

A High Energy Density Solar Rechargeable Redox Battery†

Mohammad Ali Mahmoudzadeh*[a], Ashwin R. Usgaocar[a], Joseph Giorgio[b], David L. Officer[b], Gordon G. Wallace[b] and John D.W. Madden[a]

Received Xth XXXXXXXXXX 20XX, Accepted Xth XXXXXXXXX 20XX
First published on the web Xth XXXXXXXXXX 200X
DOI: 10.1039/b000000x

An integrated solar energy conversion and storage system is presented using a dye sensitized electrode in a redox battery structure. A stable discharge voltage is shown with high areal energy storage capacity of 180 $\mu W\,h\,cm^{-2}$ by choosing iodide/polysulfide as the pair of active materials matched with permeable porous electrodes. The solar rechargeable battery system offers a higher round-trip efficiency and potential cost savings on fabrication compared to individual devices.

1 Introduction

The global concerns over the impact of conventional energy sources on the environment have resulted in a great interest in carbon-neutral energy generation. While solar energy has the potential to supply all the global energy demand, variability during daytime and intermittency as a result of atmospheric conditions are hindering its widespread use. Therefore, large-scale electrical energy storage systems are required to balance the grid during intermittency.

A solar power rechargeable battery could lead to cost and space efficiency and reduce the complexity of solar energy harvesting systems. Several attempts have been made to achieve such a device starting with back-to-back fabrication of the battery and solar cell[1,2]. Recently, great interest has been shown in the integration of a dye sensitized solar cell (DSSC) and a battery because of the electrochemical nature of DSSCs and their similar structure to batteries. These efforts can be classified into two groups. First, the devices where the energy storage and energy conversion materials are separated and have independent electrochemistry as shown in Fig. 1(a). The three electrode setup is achieved by using a bi-functional center electrode. These devices are in fact similar to back-to-back fabricated solar cell-battery structures and their working mechanism involves similar energy conversion steps as in the individual solar cells and batteries[3–6]. After illumination, electrons are pumped into the TiO_2 conduction band, travel through the external circuitry and reduce the active materials at the end electrode (bottom). Meanwhile in the DSSC, redox species are oxidized on the photo-electrode (top) and reduced at the center electrode. The latter electron transfer is balanced by the oxidation of the active material on the other side of the bi-functional electrode. This way, the solar energy is stored in a separate device from the DSSC. Although this method reduces some internal resistive losses, it still involves two distinct energy conversion steps, each involving a potential drop, and offers no significant performance or cost benefits over separate devices.

In the second group, which includes the current work, some active parts are shared between the energy conversion and storage devices (Fig. 1(b)). The mechanism involves fewer energy conversion steps compared to two separate devices, which could lead to improvement in solar energy storage yield (storage at a higher potential with lower Coulombic losses) and the reduction in the total device cost. The device itself of course becomes somewhat more complex. During the photo-charging, electrons flow through the external circuitry and reduce the active material at electrode C. The redox species are then oxidized on the photo-electrode and the solar energy is stored, but with the advantages of fewer parts and the possibility of less overpotential loss (since there are three electrodes instead of four)[7–10].

The first integrated DSSC-based solar battery was introduced in 2004 by Nagai and Segawa[7] using a polypyrrole electrode, together with a dye sensitized electrode, affording an areal energy density less than 0.3 $\mu W\,h\,cm^{-2}$ and self discharge time of less than 10 min. In the following years, activated carbon[3,4], tungsten oxide[8], carbon nanotubes[5] were also tested as the storage electrodes. A peak energy density of 170 $\mu W\,h\,cm^{-2}$ was later obtained with ruthenium oxide. Recently, Suzuka *et al.* reported an aqueous DSSC with polyviologen electrode in an aqueous storage enabled DSSC device[10]. A discharge voltage of ca. 0.4 V and discharge capacity of

† Electronic Supplementary Information (ESI) available: [details of any supplementary information available should be included here]. See DOI: 10.1039/b000000x/

[a] *Department of Electrical, University of British Columbia, 2332 Main Mall, Vancouver BC, V6T 1Z4, Canada. Tel: +1 6048 26267; E-mail: alim@ece.ubc.ca*
[b] *Intelligent Polymer Research Institute, ARC Centre of Excellence for Electromaterials Science, AIIM Facility, Innovation Campus, University of Wollongong, North Wollongong, NSW 2522, Australia.*

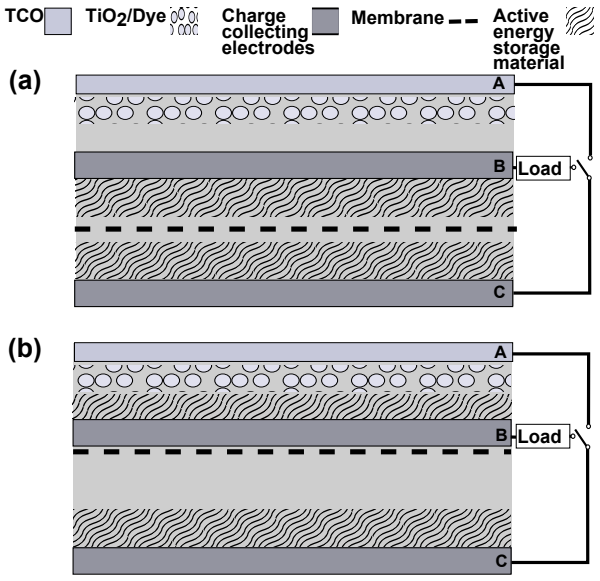

Fig. 1 Schematic of different approaches towards the integrated solar battery. The operation mode is selected by the switch.(a) Back-to-back fabricated solar cell and battery. The middle electrode is shared between the two devices.(b) Integrated solar battery. Both half cells are active during energy capture and storage. Active energy storage materials are shared between the two operation modes.

74 μA h was reported by Suzuka.

Voltage stability is an important property of power sources. A flat discharge curve means that the power source can be used with a linear regulator, while a steep-sloped curved indicates the need for a switching regulator, which is not practical for portable applications. Furthermore, a steep discharge curve means a smaller portion of the stored energy is usable. Unfortunately, all the storage-enabled DSSCs developed to date, suffer from poor voltage stability (excluding the photoassisted rechargeable batteries that only aquire part of their recharging energy from solar energy[6]).

In this work, a viable solution for the solar-battery integration challenge is demonstrated; a solar redox battery with the highest reported charge density, energy capacity and the most stable discharge voltage based on iodide/polysulfide redox couples using electro-catalytic porous electrodes. An energy density per electrode area of 180 $\mu W h cm^{-2}$ is achieved with a flat discharge voltage of less than 0.5 mV drop in 1 percent discharge, which is 5 times more stable than any other integrated solar energy harvesting and storage device.

2 Design

The solar rechargeable redox battery was designed by adding a porous dye-sensitized electrode to the redox battery structure. This resulted in a DSSC-like half cell in a battery, as depicted in Fig. 2. In this design, during illumination and charging the sensitized electrode is connected to the reduction electrode in the other half cell via a switch, causing the oxidation of ions in the DSSC and reduction in the second half cell. A charge balancing ion (shown as $\oplus$) balances the charge across the two half cells by transport through the membrane. The stored energy could later be extracted through the two non-sensitized electrodes after switching to discharge mode (middle and right in Fig. 2).

The device was demonstrated by showing the photocharge/discharge response of the cell. It involved identifying the proper redox couples and optimizing the physical parameters for efficient performance as both a solar cell and a battery. The complete cell was assembled in a sandwich structure and was tested for efficiency, cycle life and energy capacity. The integrated device has the potential to be extended to a solar redox flow battery (RFB) by adding a flow mechanism to the current redox battery.

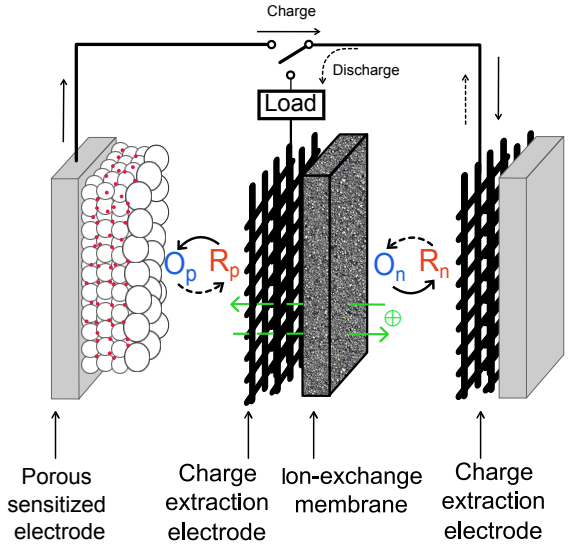

Fig. 2 Schematic of a solar chargeable redox battery. Solid arrows show the electron flow direction during photocharging and dashed arrows represent the discharge.

2.1 Redox couples

The photosensitive half-cell electrolyte should have excellent compatibility with the sensitized electrode to maximize the solar energy conversion. A review of the DSSC literature shows that very few redox couples can be effectively used as mediators in a DSSC structure. In order to achieve a highly efficient DSSC, the redox mediator should have an electrochemical potential close to the HOMO of the sensitizing dye, slow

kinetics of back electron transfer (recombination) from TiO_2, a fast kinetic rate with the charge extraction counter electrode, a high diffusion coefficient to minimize mass transport losses, low light absorption in order not to compete with the dye and good stability and interaction with the metal electrodes. Energy storage additionally requires the redox couple to be highly soluble in order to allow for high energy capacity. It is also important that a separator could be found that prevents cross-over of the redox couples between the two half-cells.

The iodide/triiodide couple is chosen as the active component of the positive electrolyte. It has proven to be one of the most effective mediators for DSSCs [11]. It also has a a higher solubility, and thus a higher capacity, compared to cobalt-based mediators, which are the other effective redox group used in DSSC fabrication.

The anodic redox couple should once again have high solubility and be separable from the other redox couple with the use of a selective membrane. It should also have a standard potential close to the TiO_2 conduction band. It was reasonable to look at the redox couples that have been shown to be practical in redox batteries as they already have satisfied most of the mentioned prerequisites. Some of these redox couples with feasible redox potentials are depicted in Fig. 3. Among these, polysulfide (S_4^{2-}/S_2^{2-}) has been selected because of its standard potential, which is close to the conduction band edge in TiO_2, its fast electron transfer rate, high solubility, its high stability and the fact that cross contamination could be avoided by using a cationic exchange membrane (CEM) if coupled with the iodide/triiodide half cell. In fact, polysulfide has been widely used together with bromine, an element right above iodine in the periodic table, as a high energy density RFB [12].

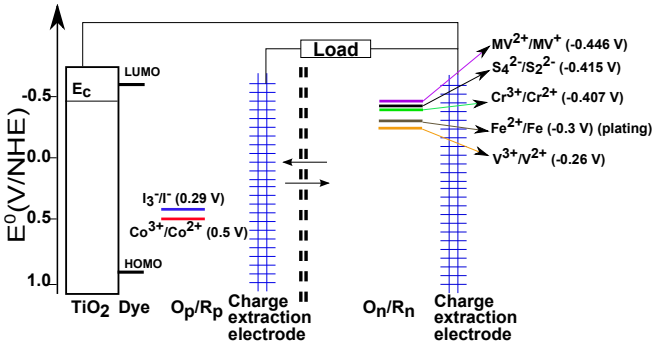

Fig. 3 Energy diagram of Redox couples for the solar redox battery. The energy levels of the TiO_2 electrode, ruthenium dye (HOMO and LUMO), and well established DSSC mediators are shown on the left hand side of the cell. On the right hand side of the membrane (vertical dashed line), candidate redox couples for completing the cell are shown with their respective standard potentials.

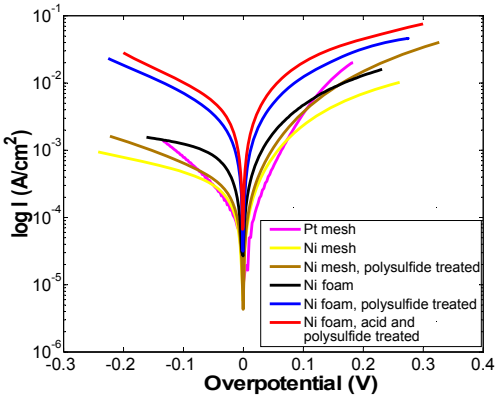

Fig. 4 Tafel plots of several electrodes towards the polysulfide redox couples. The electrolyte is 1 M Na_2S_4, 1 M $NaClO_4$ in AcN/THF (2:1 v/v). The scan rate is $10\,mV\,s^{-1}$. The horizontal line at $10\,mA\,cm^{-2}$ represents the expected operating current density of the device, at which point overpotential should be minimized. Nickel foam is seen to enable good current density with a relatively small overpotential (< 200 mV).

2.2 Electrodes

A platinum mesh was used as the positive electrode for the cell demonstration. Finding a charge extracting electrode to interact with polysulfide needed further experiments and a comparison of the materials' activity towards the polysulfide redox couple. The activity was measured using a potentiodynamic sweep around the redox potential of the respective redox couple. It was assumed that in each experiment the electrode's current was Faradaic and was only sourced from the reaction with the active species. A reasonable design goal for energy conversion and storage applications is an electrode with current densities on the order of $10\,mA\,cm^{-2}$ and an overpotential smaller than 100 mV [13]. The design in this work also required the electrode to be permeable to the electrolyte. A literature survey showed that polysulfide electrolytes have been commonly used for electrochemical cells such as the Na-S batteries [14], bromine-polysulfide redox flow batteries [12], semiconductor/liquid junction solar cells [15] and lithium-dissolved polysulfide batteries [16]. Materials such as MoS_2, Ni, Co, NiS, PbS [17], WC [18], WS_2 [19] and a variety of carbons [20] have been suggested as highly catalytic electrodes for polysulfide. Based on their reported performance, it was decided to investigate Ni, NiS and Pt electrodes as the anode. The activities of these electrodes were investigated and are depicted in Fig. 4.

The highest activity is observed from the acid treated, sulfurated Ni foam electrode. A set of experiments was performed to maximize the electrocatalytic activity of this electrode by changing acid and polysulfide treatment times. The Tafel parameters of these electrodes are extracted by fitting the polarization data to the exponential Tafel behavior of the

Butler-Volmer model, $i = i_0 \times 10^{\pm\eta/b}$, where i is the electrode current, i_0 is the exchange current density, η is the overpotential and b is the Tafel slope that can be different for anodic and cathodic branches. Average anodic and cathodic exchange current densities for Ni foam samples with different treatment times of acid and polysulfide are plotted in Figure 5(a). The activity increases with polysulfide treatment time up to 120 min and reaches a plateau around that time. It can also be seen in 5(a) that long acid exposure time has an adverse effect on exchange current densities, mainly due to the corrosion of the porous metal.

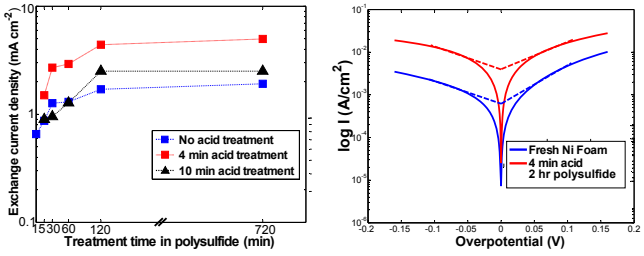

(a) (b)

Fig. 5 (a) Average anodic and cathodic exchange current densities for Ni foam samples with different treatment times of acid and polysulfide. (b) Tafel plots of fresh vs. treated Ni foam electrodes. The electrolyte is 1 M Na_2S_4, 1 M $NaClO_4$ in AcN/THF (2:1 v/v). The scan rate is 1 mV s^{-1}.

The Tafel parameters of the Ni foam electrode with the best performance are compared to fresh Ni foam and listed in Table 1. Although the larger than 120 mV decade^{-1} anodic and cathodic Tafel slopes do not represent a purely kinetically controlled reaction, the exchange current density of ~ 4 mA cm^{-2} demonstrated in the actual foam is sufficient to handle the photo-generated current with insignificant polarization loss. At 100 mV overpotential, the activated electrode drives 17 mA cm^{-2} and 14 mA cm^{-2} anodic and cathodic currents, respectively.

Table 1 Polarization of Ni foam electrodes in polysulfide electrolyte.

Electrode		Anodic	Cathodic
	i_0 (mA cm^{-2})	b(mV decade^{-1})	b(mV decade^{-1})
Ni foam, fresh	0.62	110	188
Ni foam, activated	4	155	185

2.3 Electrolyte solvent

Another component that should be mutually compatible between the DSSC and the battery is the electrolyte solvent. Aqueous electrolytes are most commonly used for redox flow batteries and the use of non-aqueous electrolytes is normally limited to high voltage batteries where water electrolysis could disrupt device performance. However, water-based DSSCs are not very promising at the moment because of dye detachment, formation of iodate, and a decrease in lifetime of the photoexcited electrons[21]. Low viscosity, polar organic solvents such as acetonitrile (AcN), ethylene carbonate (EC), propylene carbonate (PC) and methoxypropionitrile (MPN) are typically used for ruthenium dye-based DSSCs[11]. However, polysulfide solubility in PC, EC and MPN is reported to be less than 0.1 M[22], which is not practical for a redox battery because it results in a very low energy density. Initially, we tested AcN as solvent for an iodine/polysulfide redox battery but it showed very poor rechargeability characteristics. The reason was found to be the limited solubility of small chain polysulfide anions in AcN. Other than water, only tetrahydrofuran (THF)[16], and a mixture of dimethoxy ethane (DME) and 1,3-dioxolane (DOL) (1:1 v/v) [23,24] have been reported to have high solubilities of polysulfides (~ 10 M). Although neither of them has been utilized in a DSSC device, a mixture of THF in AcN is reported to have a positive effect on DSSC performance at up to a 30% volumetric ratio of THF in AcN[25]. As a result, an AcN/THF (2:1 v/v) mixture was used in this work to simultaneously address the high redox solubility need of a redox battery and low viscosity, high polarity requirements of DSSCs.

Considering all the design requirements, a material set suitable for an integrated solar redox battery was selected and is listed in Table 2. The half-cell reactions are

$$3I^- \underset{\text{discharge}}{\overset{\text{charge}}{\rightleftharpoons}} I_3^- + 2e^- \qquad \text{(cathode)}, \qquad (1)$$

$$S_4^{2-} + 2e^- \underset{\text{discharge}}{\overset{\text{charge}}{\rightleftharpoons}} 2S_2^{2-} \qquad \text{(anode)}, \qquad (2)$$

and the net reaction with Na^+ as the charge balancing ion is

$$3NaI + Na_2S_4 \underset{\text{discharge}}{\overset{\text{charge}}{\rightleftharpoons}} NaI_3 + 2Na_2S_2 \qquad \text{(net)}, \qquad (3)$$

that leads to a cell open circuit voltage of *ca.* 0.7 V, close to the difference in electrochemical potentials of S_4^{2-}/S_2^{2-} (−0.415 V vs. NHE[26]) and I_3^-/I^- (0.29 V vs. NHE[27]).

Performance was first investigated in an iodide-polysulfide redox battery structure without the inclusion of photocharging. Upon verification of reversible electrochemistry and the stability of electrolytes, the complete system was assembled and characterized. The results of these tests are presented in the next section followed by the details of the experimental procedures.

Table 2 List of materials for an efficient, high energy density solar redox battery.

Device part	Material
Photoelectrode	15 μm TiO_2 sensitized with N719 dye
Positive electrode	Pt Mesh
Positive electrolyte	1 M I_2, 0.1 M NaI, 1 M $NaClO_4$ in AcN/THF (2:1 v/v)
Negative electrode	Ni foam, acid/polysulfide pre-treated
Negative electrolyte	1 M Na_2S, 3 M S, 1 M $NaClO_4$ in AcN/THF (2:1 v/v)
Membrane	CMI-7000 cationic exchange membrane

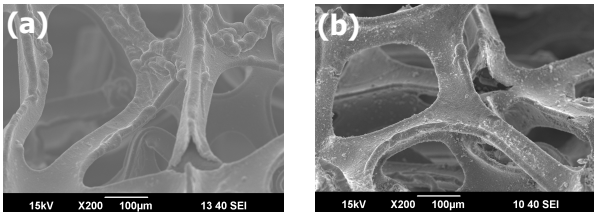

Fig. 6 SEM images of the Ni foam, (a) before and (b) after treatment with acid and polysulfide.

3 Experimental

3.1 Electrochemical cell preparations

Sodium sulfide nonahydrate, ($Na_2S \cdot 9\,H_2O$, 98.0 %), sulfur, sublimed (S, 99.5.0%), iodine, resublimed (I_2, 99.5.0%), sodium iodide (NaI), sodium hydroxide pellets (NaOH, 97%) were purchased from Fisher Scientific. Sodium perchlorate ($NaClO_4$, 98%), acetonitrile anhydrous (CH_3CN, 99.8%) were supplied from Sigma Aldrich. Tetrahydrofuran (C_4H_8O, 99.99%) is obtained from EMD Millipore Chemicals. Nickel (Ni foam, 99.99%) was purchased readily from MTI Corporation. The ion exchange membrane CMI-7000 was supplied by Membrane International.

The conductive glass of the sensitized electrode is fluorine doped tin oxide coated with a resistance of 8 Ω/sq and was purchased from Solaronix. The sensitizing dye, Ruthenizer 535 bis-TBA dye (N719) was purchased from Dyesol.

The electrochemical glassware was washed with 2 % Extran 3000 in water solution followed sonication in ethyl alcohol and acetone.

The DSSC/positive half-cell electrolyte was prepared by dissolving appropriate weights of materials for a 1 M NaI, 0.1 M I_2 and 1 M $NaClO_4$ solution in AcN/THF (2:1 v/v). The mixture was stirred for 2 h.

In order to prepare the negative electrolyte, initially, 3 M sodium sulfide was dissolved in THF by stirring and warming the solution to 40 °C. Sulfur was then added in three times the concentration of Na_2S. The mixture was heated to 50 °C and stirred at 400 RPM for 2 h before it changed color from a light yellow to brownish red. After a uniform solution was achieved, additional solvent was added to maintain 3 M solution on Na_2S_4. Then ($NaClO_4$) was added in 3 M concentration. Finally, the solution was diluted with AcN to produce a 1 M solution of Na_2S_4 in AcN/THF (2:1 v/v).

The pre-treated Ni foam electrode was prepared by first immersing a piece of Ni foam in a clean (1:1 v/v) sulfuric acid/water solution for 4 min. After rinsing with DI water, the electrode was boiled in DI water for 1 min and then was boiled in 1 M aqueous solution of Na_2S_4 (prepared similar to the negative half-cell electrolyte) for 2 h. The electrodes were boiled in DI water for another 1 min and then dried under vacuum at 60 °C. SEM images of the fresh and activated Ni foam are shown in Fig. 6. NiS layer is shown as clusters on the smooth surface of Ni.

In order to adjust the membrane for the non-aqueous solvent, it was immersed in 1 M Na_2ClO_4 in AcN/THF (2:1 v/v). The container was then held under vacuum to enforce the substitution of air with the solvent. The membranes was then stored in the same electrolyte for 24 h. An EIS study of the membranes showed an ionic resistance of 240 Ωcm^2. Another CEM from Fumatech GmbH (FKB PK130) with a reported resistance of $< 4\,\Omega cm^2$ in aqueous electrolyte was also tested because of previous reports on its application in non-aqueous RFBs[28]. The latter, however, showed a much higher ionic resistance in the solvent in this work (AcN/THF (2:1 v/v)) compared to CMI-7000 which was used in these experiments as reported in the supplementary information.

For the photoelectrode, the technique explained by Ito *et al.*[29] was followed for most of the electrode preparation. First, two holes were drilled in FTO coated glass electrodes using two sacrificial glass layers on top and bottom to avoid chipping the glass surface during the drilling. Then the FTO coated glass electrodes were cleaned in a sonication bath with soapy water, followed by an acetone and ethanol wash. The sonication time for each step was 20 minutes. The electrodes were then dried and heated to 450 °C before spraying with titanium diisopropoxide bis(acetylacetonate) solution 75 % (Aldrich) in absolute ethanol with volume ratio 1:9. A 43T screen printing process was then used to deposit TiO_2 nanoparticles (Dyesol, 18NR-T) with a thickness of 12 μm and then sintering stepwise using a programmable hot plate with a maximum temperature of 500 °C. A thin layer of TiO_2 was deposited on the electrodes by immersing the electrodes in 20 mM aqueous solution of $TiCl_4$ kept at 70 °C for 30 minutes. The electrodes were then slowly reheated to 500 °C and held for 30 minutes. The cooled electrodes are sensitized in 0.5 mM solution of N719 in a 1:1 volume mixture of acetonitrile and tert-butyl alcohol for 24 h.

3.2 Electrochemical and Photoelectrochemical measurements

All the cyclic voltametries and I-V characteristics were carried out using a PGSTAT101 Autolab potentiostat in a 2 electrode setup. The solar redox battery was tested in the sandwich cell of Fig. 7. For charging, the photoelectrode and anode were directly connected and the discharging happened at a constant current of $0.2\,\mathrm{mA\,cm^{-2}}$.

The light source was a Newport 150 W Xenon arc lamp coupled to a filter (AM 1.5D), driven by a Newport 69907 power supply (Newport Inc., Irvine CA). The output power was measured using a Newport 818-SL photodetctor and was adjusted at $100\,\mathrm{mW\,cm^{-2}}$.

4 Results

High energy density and Coulombic efficiency combined with device stability and cycle life are the prerequisites of any battery. A solar-battery should also have high energy conversion efficiency. These characteristics were investigated in the solar redox battery and discussed below. Several cells are fabricated and analyzed. Performance was within 15 % for all the tests. Here the results from the best performing cell are reported as these provide the clearest indication of the potential of this new, un-optimized approach.

4.1 DSSC performance

In order to ascertain DSSC performance, in the procedure used the DSSC is tested using the positive electrolyte prescribed for the battery. The electrode separation was set to 0.3 mm to mimic that of the solar-battery structure. The IV characteristics and short circuit current are depicted in Fig. 8(a). The efficiency of the DSSC was measured to be $\sim 1.7\,\%$. This was expected due to the diffusion limited current at the selected electrode separation. In future, smaller spacings enabled by fabrication processes operating with higher tolerances should boost the efficiency by allowing a thinner bulk thickness.

4.2 Solar redox battery charge/discharge

The solar rechargeable redox flow battery is assembled in a sandwich structure as shown in Fig. 7 using the components identified in the previous sections. The window and the spacer openings were set to $1\,\mathrm{cm^2}$ and the thickness of the spacers was $300\,\mu\mathrm{m}$.

Photocharge/discharge characteristics of the solar redox battery are shown in Fig. 8(b). At the onset of discharge, the cell voltage drops instantly for $100\,\mathrm{mV}$ because of ohmic losses in the membrane and the electrodes. Throughout the discharge, a Nernstian dependency is observed between the voltage and state of discharge (SOD) of the cell. A complete discharge test is performed to measure the capacity of the cell.

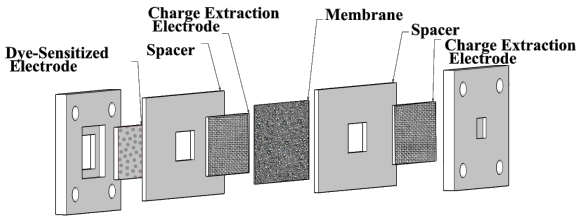

Fig. 7 Solar redox battery sandwich structure

A comparison of the results of the solar redox battery of this work with the previous DSSC-based solar battery devices is presented in Table 3. With an areal energy density of $180\,\mu\mathrm{W\,h\,cm^{-2}}$, this work presents the highest areal energy density among solar batteries. More importantly, the iodide/polysulfide solar battery produced the highest quality voltage with a drop less than 0.5 mV per 1 percent discharge. This presents a discharge curve at least 10 times flatter than those of the other storage-enabled DSSCs. Fig. 8(d) shows the cell energy round-trip efficiency, which starts at more than 98 % and gradually drops to 78 % after 3 cycles, stabilizing at just above this value over the following 7 cycles. While this efficiency decrease may be due to an initial solvent loss, a variety of other factors may also contribute such as dye desorption into the electrolyte, binding of electrolyte components to cell surfaces, and change in electrode surfaces on cycling. This efficiency loss requires further investigation and cell optimization. However, the efficiency stabilization over the last seven cycles bodes well for the long term stability of this device.

The cycling results for the redox battery alone, show great stability of the discharge voltage and near perfect round-trip efficiency and preservation of the energy over 50 cycles as reported in the supplementary information document.

For separate PV panels and batteries, the electrical energy storage efficiency is $\sim$ 40-56 % for AC output and $\sim$ 49-62 % for DC output power[30]. Comparison of the latter value with the energy storage efficiency of the combined solar redox battery supports our initial expectation about reduction of energy conversion losses in an integrated solar cell-battery device.

5 Conclusion

A solar rechargeable redox battery is demonstrated and a set of materials is proposed for achieving an efficient device. It shows the highest performance yet achieved in any integrated DSSC-based energy storage device. Significant improvement in the areal and volumetric capacity is observed compared

Table 3 Performance comparison of DSSC-based solar batteries.

Areal energy density ($\mu W h cm^{-2}$)	Areal discharge capacity ($\mu A h cm^{-2}$)	Initial discharge voltage (V)	Discharge slope (mV/% SOD)[a]	Photo-conversion efficiency (%)	Roundtrip efficiency (%)	Coulombic efficiency (%)	Ref
9.3	76.38	0.45	NR[b]	NR[b]	NR[b]	80	3
47	130	0.75	5.7	NR[b]	NR[b]	42	4
20	41	0.7	3.05	NR[b]	NR[b]	36	8
21	54	0.75	8	6.10	84	∼100	5
170	400	0.88	8.8	0.8	NR[b]	∼88	31
3.5	8.3	0.6	3.9	NR[b]	NR[b]	NR[b]	32
27	74	0.55	2.1	1.3	NR[b]	95	10
180	240	0.8	0.4	1.7	78	∼ 100	This work

[a] Voltage drop over one percent discharge for a 75 % charged cell (mV/ %)
[b] Not reported

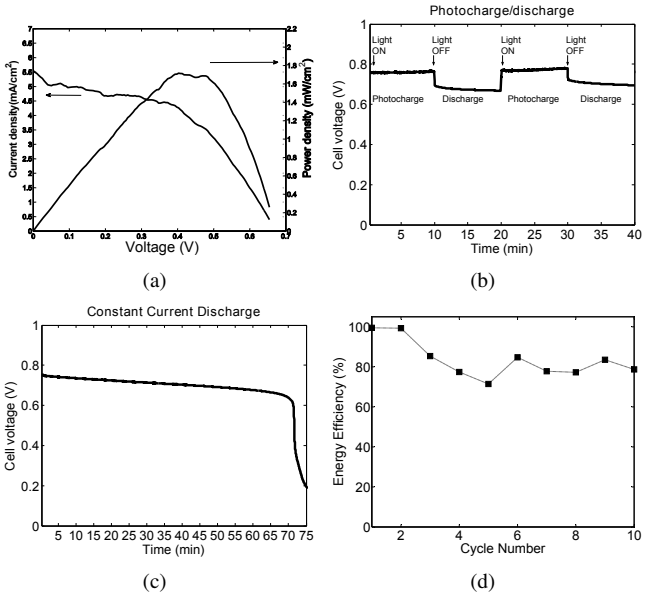

Fig. 8 (a) IV characteristics and short circuit current of DSSC using the solar-battery electrolyte (1 M I_2, 0.1 M NaI, 1 M $NaClO_4$ in AcN/THF (2:1 v/v)).(b) Photocharge / Discharge and, (c) complete discharge of the solar redox battery. (d) Energy efficiency during charge/discharge cycles. For charging, the photoelectrode and anode are directly connected and the discharging is at a constant current of $0.2\,mA\,cm^{-2}$.

to the only other combined solar rechargeable redox battery demonstrated to date. The tests suggest that the cell-thickness dependency of the DSSC performance is the main factor limiting performance. This effect could be markedly reduced in a flow cell where the supply of iodide to the photoelectrode was provided by convection from external sources rather than diffusion. Further improvement of the photoelectrode, membrane and charge extraction electrodes should also result in more efficient performance.

6 Acknowledgments

The authors gratefully acknowledge the financial support through Discovery and Strategic Grants from the Natural Sciences and Engineering Research Council (NSERC) of Canada and The Peter Wall Institute for Advanced Studies at UBC. Funding from the Australian Research Council Centre of Excellence scheme (Project Number CE 140100012) is gratefully acknowledged. The authors would like to thank the Australian National Nanofabrication Facility Materials Node for equipment use.

References

1 G. Dennler, S. Bereznev, D. Fichou, K. Holl, D. Ilic, R. Koeppe, M. Krebs, A. Labouret, C. Lungenschmied, A. Marchenko, D. Meissner, E. Mellikov, J. Mot, A. Meyer, T. Meyer, H. Neugebauer, A. pik, N. S. Sariciftci, S. Taillemite and T. Whrle, *Solar Energy*, 2007, **81**, 947–957.

2 G. Wee, T. Salim, Y. M. Lam, S. G. Mhaisalkar and M. Srinivasan, *Energy & Environmental Science*, 2011, **4**, 413–416.

3 T. Miyasaka and T. N. Murakami, *Applied Physics Letters*, 2004, **85**, 3932–3934.
4 T. N. Murakami, N. Kawashima and T. Miyasaka, *Chemical Communications*, 2005, 3346–3348.
5 Z. Yang, L. Li, Y. Luo, R. He, L. Qiu, H. Lin and H. Peng, *Journal of Materials Chemistry A*, 2012, **1**, 954–958.
6 M. Yu, X. Ren, L. Ma and Y. Wu, *Nature Communications*, 2014, **5**, 5111.
7 H. Nagai and H. Segawa, *Chemical Communications*, 2004, **8**, 974–975.
8 Y. Saito, S. Uchida, T. Kubo and H. Segawa, *ECS Transactions*, 2009, **16**, 27–34.
9 Y. Saito, A. Ogawa, S. Uchida, T. Kubo and H. Segawa, *Chemistry Letters*, 2010, **39**, 488–489.
10 M. Suzuka, S. Hara, T. Sekiguchi, K. Oyaizu and H. Nishide, *Polymer*, 2015, **68**, 353–357.
11 S. Feldt, *dissertation*, Uppsala University, 2013.
12 R. J. Remick and P. G. P. Ang, *US patent*, 1984, US4485154 A.
13 P. M. Lessner, F. R. McLarnon, J. Winnick and E. J. Cairns, *Journal of Applied Electrochemistry*, 1992, **22**, 927–934.
14 K. M. Abraham, R. D. Rauh and S. B. Brummer, *Electrochimica Acta*, 1978, **23**, 501–507.
15 S. Licht, R. Tenne, H. Flaisher and J. Manassen, *Journal of The Electrochemical Society*, 1986, **133**, 52–59.
16 R. D. Rauh, K. M. Abraham, G. F. Pearson, J. K. Surprenant and S. B. Brummer, *Journal of The Electrochemical Society*, 1979, **126**, 523–527.
17 Z. Tachan, M. Shalom, I. Hod, S. Ruhle, S. Tirosh and A. Zaban, *The Journal of Physical Chemistry C*, 2011, **115**, 6162–6166.
18 D. V. Esposito, K. D. Dobson, B. E. McCandless, R. W. Birkmire and J. G. Chen, *Journal of The Electrochemical Society*, 2009, **156**, B962–B969.
19 I. E. L. Stephens, C. Ducati and D. J. Fray, *Journal of The Electrochemical Society*, 2013, **160**, A757–A768.
20 H. Zhou, H. Zhang, P. Zhao and B. Yi, *Electrochimica Acta*, 2006, **51**, 6304–6312.
21 C. Lal, *Journal of Power Sources*, 2007, **164**, 926–930.
22 R. D. Rauh, F. S. Shuker, J. M. Marston and S. B. Brummer, *Journal of Inorganic and Nuclear Chemistry*, 1977, **39**, 1761–1766.
23 Y. Fu, Y. S. Su and A. Manthiram, *Angewandte Chemie International Edition*, 2013, **52**, 6930–6935.
24 Y. Yang, G. Zheng and Y. Cui, *Energy & Environmental Science*, 2013, **6**, 1552–1558.
25 A. Fukui, R. Komiya, R. Yamanaka, A. Islam and L. Han, *Solar Energy Materials and Solar Cells*, 2006, **90**, 649–658.
26 N. S. A. Manan, L. Aldous, Y. Alias, P. Murray, L. J. Yellowlees, M. C. Lagunas and C. Hardacre, *The Journal of Physical Chemistry B*, 2011, **115**, 13873–13879.
27 G. Boschloo and A. Hagfeldt, *Accounts of Chemical Research*, 2009, **42**, 1819–1826.
28 S.-H. Shin, S.-H. Yun and S.-H. Moon, *RSC Advances*, 2013, **3**, 9095–9116.
29 S. Ito, P. Chen, P. Comte, M. K. Nazeeruddin, P. Liska, P. Pchy and M. Gratzel, *Progress in Photovoltaics: Research and Applications*, 2007, **15**, 603–612.
30 V. C. Nelson, *Introduction to Renewable Energy*, CRC Press, Boca Raton, FL, 1st edn, 2011.
31 M. Skunik-Nuckowska, K. Grzejszczyk, P. J. Kulesza, L. Yang, N. Vlachopoulos, L. Hggman, E. Johansson and A. Hagfeldt, *Journal of Power Sources*, 2013, **234**, 91–99.
32 N. Yan, G. R. Li and X. Gao, *Journal of The Electrochemical Society*, 2014, **161**, A736–A741.

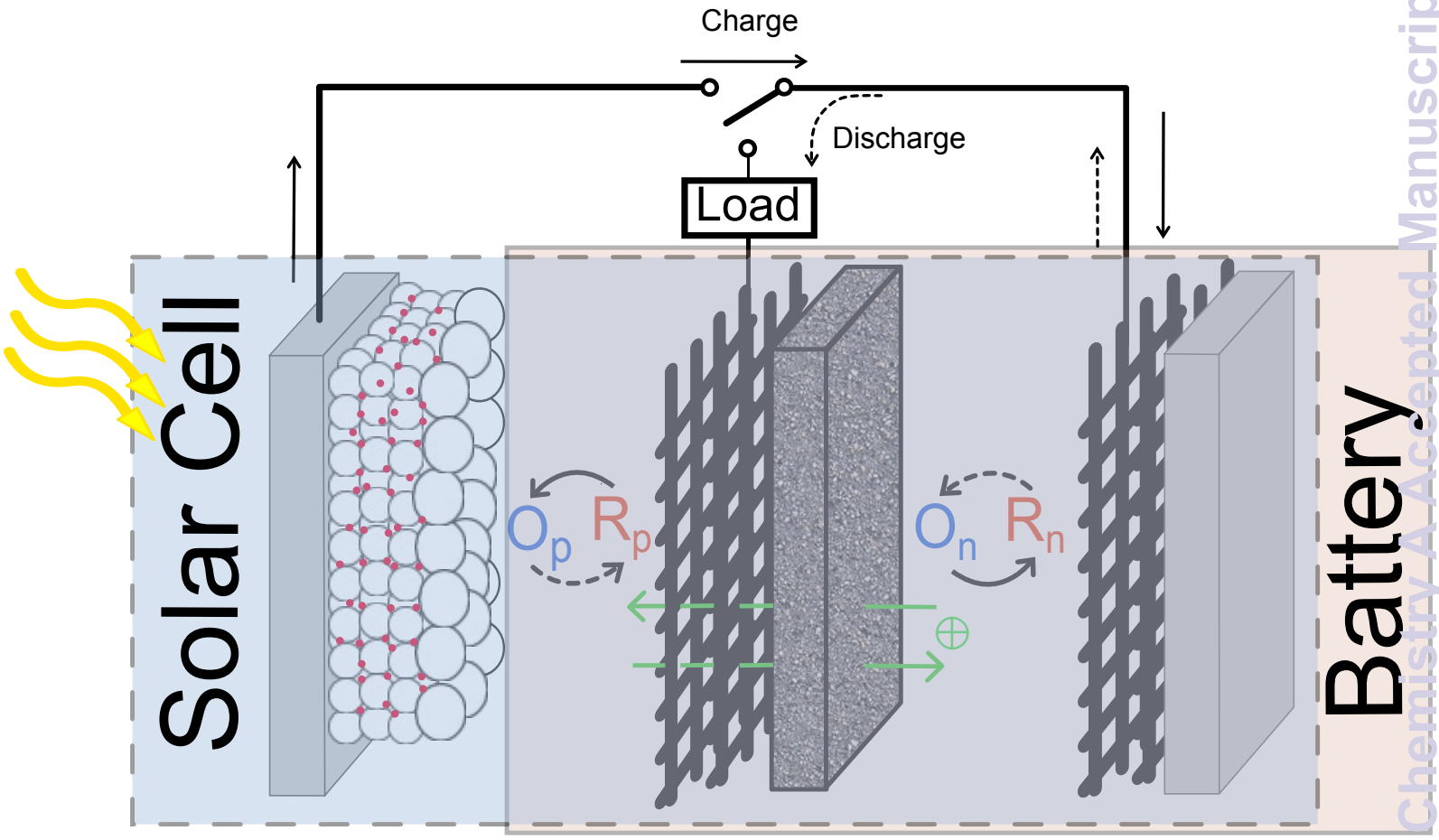

An integrated solar energy conversion and storage system is presented using a dye sensitized electrode in a redox battery structure.